



**EUROfusion**

EUROFUSION WPJET1-PR(15) 13755

CF Maggi et al.

## **Pedestal confinement and stability in JET-ILW ELMy H-modes**

Preprint of Paper to be submitted for publication in  
Nuclear Fusion



This work has been carried out within the framework of the EUROfusion Consortium and has received funding from the Euratom research and training programme 2014-2018 under grant agreement No 633053. The views and opinions expressed herein do not necessarily reflect those of the European Commission.

This document is intended for publication in the open literature. It is made available on the clear understanding that it may not be further circulated and extracts or references may not be published prior to publication of the original when applicable, or without the consent of the Publications Officer, EUROfusion Programme Management Unit, Culham Science Centre, Abingdon, Oxon, OX14 3DB, UK or e-mail [Publications.Officer@euro-fusion.org](mailto:Publications.Officer@euro-fusion.org)

Enquiries about Copyright and reproduction should be addressed to the Publications Officer, EUROfusion Programme Management Unit, Culham Science Centre, Abingdon, Oxon, OX14 3DB, UK or e-mail [Publications.Officer@euro-fusion.org](mailto:Publications.Officer@euro-fusion.org)

The contents of this preprint and all other EUROfusion Preprints, Reports and Conference Papers are available to view online free at <http://www.euro-fusionscipub.org>. This site has full search facilities and e-mail alert options. In the JET specific papers the diagrams contained within the PDFs on this site are hyperlinked

# Pedestal Confinement and Stability in JET-ILW ELMy H-modes

C.F. Maggi<sup>1</sup>, S. Saarelma<sup>1</sup>, F.J. Casson<sup>1</sup>, C. Challis<sup>1</sup>, E. de la Luna<sup>2</sup>, L. Frassinetti<sup>3</sup>,  
C. Giroud<sup>1</sup>, E. Joffrin<sup>4</sup>, J. Simpson<sup>1</sup>, M. Beurskens<sup>1</sup>, I. Chapman<sup>1</sup>, J. Hobirk<sup>5</sup>, M. Leyland<sup>6</sup>,  
P. Lomas<sup>1</sup>, C. Lowry<sup>7</sup>, I. Nunes<sup>8</sup>, F. Rimini<sup>1</sup>, A.C.C. Sips<sup>7</sup>, H. Urano<sup>9</sup> and JET Contributors\*

*EUROfusion Consortium, JET, Culham Science Centre, Abingdon, OX14 3DB, UK*

<sup>1</sup>*CCFE, Culham Science Centre, Abingdon OX14 3DB, UK*

<sup>2</sup>*Asociacion CIEMAT, Madrid, Spain*

<sup>3</sup>*Association VR, Fusion Plasma Physics, KTH, SE-10044 Stockholm, Sweden*

<sup>4</sup>*CEA, IRFM, F-13108 Saint-Paul-lez-Durance, France*

<sup>5</sup>*Max-Planck-Institut für Plasmaphysik, Boltzmannstrasse 2, D-85748, Garching, Germany*

<sup>6</sup>*York Plasma Institute, Department of Physics, University of York, York YO10 5DD, UK*

<sup>7</sup>*European Commission, B1049 Brussels, Belgium*

<sup>8</sup>*Associação IST, Instituto Superior Técnico, Av Rovisco Pais, 1049-001 Lisbon, Portugal*

<sup>9</sup>*Japan Atomic Energy Agency, 801-1 Muro-yama, Naka, Ibaraki 311-0193, Japan*

\**See the Appendix of F. Romanelli et al., Proc. 25<sup>th</sup> IAEA FEC 2014, St Petersburg, Russian Federation*

*Email contact of main author: [costanza.maggi@ccfe.ac.uk](mailto:costanza.maggi@ccfe.ac.uk)*

**Abstract.** New experiments in 2013-2014 have investigated the physics responsible for the decrease in H-mode pedestal confinement observed in the initial phase of JET-ILW operation (2012 Experimental Campaigns). The effects of plasma triangularity, global beta and neutrals - both D and low-Z impurities - on pedestal confinement and stability have been investigated systematically. The stability of JET-ILW pedestals is analysed in the framework of the Peeling-Ballooning model and the pedestal predictive code EPED. Low D neutrals content in the plasma, achieved either by low D<sub>2</sub> gas injection rates or by divertor configurations with optimum pumping, and high beta are necessary conditions for good pedestal (and core) performance. In such conditions the pedestal stability is consistent with the Peeling-Ballooning paradigm. Moderate to high D<sub>2</sub> gas rates, required for W control and stable H-mode operation with the ILW, lead to increased D neutrals content in the plasma and additional physics in the pedestal models may be required to explain the onset of the ELM instability. The physics mechanism leading to the beneficial increase in pedestal temperature with N<sub>2</sub> seeding in high triangularity JET-ILW H-modes is not yet understood. The changes in H-mode performance associated with the change in JET wall composition from C to Be/W point to D neutrals and low-Z impurities playing a role in pedestal stability, elements which are not currently included in pedestal models. These aspects need to be addressed in order to progress towards full predictive capability of the pedestal height.

## 1. Introduction

The first JET experiments with the Be/W ITER-like wall (JET-ILW, MkII-HD divertor geometry, 2011-2012 campaigns) showed a reduction in the low beta ( $\beta_N \sim 1.2$ ) ELMy H-mode operation space with good confinement,  $H_{98(y,2)} \sim 1$  (where  $H_{98(y,2)} = \tau_E / \tau_{IPB98(y,2)}$ ): the confinement loss was predominantly found in the pedestal, as the pedestal temperature,  $T_{PED}$ , was reduced at all densities, while core pressure profile peaking was largely unchanged. In addition, higher H-mode performance generally obtained at high triangularity ( $\delta$ ), through improved edge stability with higher plasma shaping, appeared to have been lost: similar

pedestal pressure,  $p_{\text{PED}}$ , was observed at low and high  $\delta$  in JET-ILW at low  $\beta_{\text{N}}$  [1]. However, an unexpected but positive feature of high  $\delta$  baseline H-modes was the increase in pedestal pressure with  $\text{N}_2$  seeding - used as a tool for divertor heat load mitigation - allowing confinement factors similar to those of JET-C discharges (with the current MkII-HD divertor geometry) to be recovered [2]. In particular,  $\text{N}_2$  seeding was found to increase  $T_{\text{e,PED}}$  in JET-ILW to values approaching those of JET-C at similar  $n_{\text{e,PED}}/n_{\text{GW}}$ , while core confinement was not improved, as pressure peaking remained unaffected by  $\text{N}_2$  seeding.

When assessing the edge stability of JET ELMy H-mode plasmas, JET-C pedestals are typically found to be close to the Peeling-Ballooning (P-B) limit before a type I ELM crash, while JET-ILW H-modes at low beta ( $< 1.5$ ) and high  $\text{D}_2$  gas injection rates (without  $\text{N}_2$  seeding) were found deep in the stable region [3], primarily due to the lower  $T_{\text{e,PED}}$  compared to JET-C. In order to address the physics responsible for the decrease in pedestal confinement in the initial phase of the JET-ILW experimental campaigns, new experiments were carried out during the 2013-2014 campaigns. The new investigations reported in this paper focus on the following aspects: i) the effect of plasma triangularity; ii) the effect of beta and iii) the effect of neutrals (both D and low-Z impurities) on JET-ILW pedestal confinement and stability, reporting on the progress achieved since the 2012 IAEA Fusion Energy Conference. The stability of JET-ILW pedestals is investigated in the framework of the P-B model [4] and the pedestal predictive code EPED [5], [6], currently the leading model for predictions of the pedestal height in ITER and DEMO. The paper is organized as follows: the effect of plasma triangularity on pedestal confinement and stability is discussed in Section 2, the effect of beta is presented in Section 3, Section 4 addresses the effect of neutrals and in Section 5 conclusions are drawn.

## 2. Effect of plasma triangularity

In JET-ILW low  $\beta_{\text{N}}$  H-modes, relatively high levels of  $\text{D}_2$  gas injection are required for W control. In these plasmas the beneficial effect of plasma shaping on pedestal confinement, commonly found in many tokamaks both experimentally and numerically (see e.g. [7]), is not observed, since low and high  $\delta$  H-modes exhibit similar pedestal pressures. Typically,  $T_{\text{e,PED}}$  is lower than in JET-C at similar values of  $n_{\text{e,PED}}/n_{\text{GW}}$  [1]. This is illustrated in the edge diagram of Figure 1 for a dataset of ELMy H-modes at 2.5MA/2.5-2.7T, with NBI input power ranging from 14 to 20 MW, comparing the JET-ILW type I ELMy discharges from the recent 2013-14 experiments (in red) with data from a  $\text{D}_2$  gas scan in JET-C (in grey) at

similar input parameters [8]. The JET-C high  $\delta$  dataset could be fuelled up to the Greenwald density while maintaining good confinement ( $H_{98(y,2)} \sim 1$ ). This was connected with a transition from pure type I ELMs to mixed type I/II ELMs at the highest densities, see Figure 2 and [9], [10], [11]. The pedestals of the JET-ILW high  $\delta$  H-modes (full red circles) are found on the same isobar as the pedestals of low  $\delta$  H-modes, which in 2013-14 could be optimized towards stable operation at lower densities than those achieved during the initial ELMy H-mode phase with ILW (see section 4.3). Moreover, the high  $n_{e,PED}$  and low  $T_{e,PED}$  values of these JET-ILW high  $\delta$  type I ELMy H-modes are similar to those of type III ELMy H-modes in JET-C, obtained at the highest gas rates of the fuelling scan. A comparison of density ramp experiments in JET-C and JET-ILW at similar  $I_p/B_T$  has also revealed a reduction in pedestal temperature at which the type I ELM regime is accessed in JET-ILW [11], possibly indicating a lower type I/type III ELM threshold than in JET-C. In addition, both the edge temperature and the loss power at which the L-H transition occurs are reduced in JET-ILW in the high density branch [12]. However, all this does not translate in a confinement benefit for type I ELMy H-modes in JET-ILW.

The physics mechanism resulting in lower  $T_{e,PED}$  in JET-ILW H-modes is not yet understood and is under investigation. However, its implication on the pedestal stability can be understood within the P-B paradigm, as illustrated graphically in the  $j$ - $\alpha$  diagram of Figure 2 (with  $j$  the edge current and  $\alpha$  the dimensionless pressure gradient,  $\alpha = (2\partial_r V)/(2\pi)^2 (V/2\pi^2 R)^{1/2} \mu_0 p'$ , where  $V$  is the volume enclosed by the flux surface,  $R$  is the major radius and  $p'$  is the pressure derivative with respect to the poloidal flux  $\psi$ ). The operational point at low  $T_{e,PED}$  (red star in the diagram) and thus high pedestal collisionality,  $\nu^*_{PED}$ , and low bootstrap current,  $j_{BS}$ , is located in the ballooning region of the stability diagram. In these conditions the P-B model predicts little or no improvement in pedestal pressure with increasing  $\delta$  due to the strong reduction in the edge bootstrap current [7]. A similar stability boundary is expected both at low and high  $\delta$  (black and red curves, respectively, in the diagram of Figure 2) as indeed is observed in the low  $\beta_N$  ( $\beta_N < 1.5$ ), low  $T_{PED}$ , JET-ILW H-mode dataset of Figure 1. In such conditions a mere increase in triangularity does not recover the pedestal height.

On the other hand, H-mode operation at high  $\beta_N$  and low  $D_2$  gas injection rates has not led to energy confinement degradation after the JET wall changeover from CFC to Be/W plasma facing components, both at low and high triangularity, as reported in [13]. Therefore, in order to separate the effect of beta from that of gas injection on pedestal confinement and stability,

new power and gas scan experiments were carried out in 2013-2014. In the next section we first address the effect of beta on the confinement and stability of JET-ILW H-mode pedestals.

### 3. Effect of beta: power scans at low D<sub>2</sub> gas injection

New power scans were carried out in the 2013-2014 campaigns with low D<sub>2</sub> gas injection rates,  $\Gamma_D \sim 2.8 \times 10^{21}$  e/s, at  $I_p = 1.4\text{MA}$ ,  $B_T = 1.7\text{T}$ , both at low ( $\delta \sim 0.2$ ) and high ( $\delta \sim 0.4$ )  $\delta$  shapes [13]. As the input power (beta) is increased in subsequent discharges, the pedestal top pressure increases rapidly both at low and high  $\delta$ , as shown in Figure 3, contributing to the weak power degradation of global energy confinement observed in JET-ILW at high beta [13]. Other factors that contribute to the good confinement observed at high beta include density peaking at low collisionality, longer fast ions slowing down time resulting in larger fast ion pressure and increased core turbulence suppression due to electromagnetic effects, as analysed in detail in [13]. Here we concentrate on the pedestal effects. The data shown in Figure 3 refer to the last 30% of the type I ELM cycle and are obtained from *mtanh* [14] fits of composite HRTS profiles over the steady time window selected for the analysis. At high  $\delta$  the increase in pedestal pressure is somewhat stronger than at low  $\delta$  (see Figure 3), as  $T_{e,\text{PED}}$  increases with power/beta at constant  $n_{e,\text{PED}}$ . At low  $\delta$  the increase in  $T_{e,\text{PED}}$  is accompanied by some reduction in  $n_{e,\text{PED}}$ , however a concomitant increase in core density peaking results in the observed weak power degradation of the total energy confinement found also at low  $\delta$  [13]. The pedestal pressure of high  $\delta$ , high  $\beta_N$  H-modes, where high  $T_{\text{PED}}$  and thus low  $v^*_{\text{PED}}$  values are achieved, is about 30% higher than at low  $\delta$ . Conversely, at low beta (higher collisionality), similar pedestal pressures are observed, a result which is consistent with the findings presented in Section 2 and shown in Figure 1 for the dataset at 2.5MA/2.7T.

As the input power is increased in the experiment, the pedestal top poloidal beta,  $\beta_{\text{pol,PED}}$ , increases while the collisionality  $v^*_{e,\text{PED}}$  decreases in a correlated fashion, as typically found in power scan experiments. In order to verify experimentally for JET-ILW the scaling of the pedestal width with  $\sqrt{\beta_{\text{pol,PED}}}$ , which is assumed in the EPED model [5],[6], the variation of the pedestal pressure width would need to be investigated in a dimensionless  $\beta_{\text{pol}}$  scan, at constant  $v^*$ ,  $\rho^*$  and  $q_{95}$ . This is work in progress. However, analysis of the electron pedestal structure of the low and high  $\delta$  power scans at low D<sub>2</sub> injection can already provide useful information regarding the scaling of the pedestal width in JET-ILW. Figure 4 indicates that the pedestal pressure width increases with pedestal poloidal beta in  $\psi$  space, especially in the dataset at high  $\delta$ , and that the trend appears to be consistent with an increase proportional to

$\sqrt{\beta_{\text{pol,PED}}}$ ). For consistency with the formulation in EPED, the pedestal pressure width is derived here as the mean of the  $T_e$  and  $n_e$  widths, evaluated separately in the last 30% of the ELM cycle, using the method described in [15]. We note that in these power scans the pedestal width increases in psi space. Within the experimental uncertainty no clear increase has been observed in real space (at the outboard midplane). Therefore the pedestal broadening in psi space can be associated with the increase in Shafranov shift, which compresses the flux surfaces at the low field side. The pedestal pressure gradient is also found to increase with beta, thus the increase in  $p_{e,\text{PED}}$  with power is due to an increase in both pedestal width and gradient with beta.

The edge stability of these pedestals was investigated with the ideal MHD stability code ELITE [4], with input the measured pre-ELM pressure profiles and using the Sauter model [16] to calculate the contribution of the bootstrap current,  $j_{\text{BS}}$ , to the total edge current.  $T_i = T_e$  is assumed (consistent with charge exchange measurements) and the line averaged  $Z_{\text{eff}}$  from visible Bremsstrahlung is used in the calculation of the main ion density (with Be the main intrinsic impurity) and  $j_{\text{BS}}$ . The analysis indicates that the pressure gradient before the type I ELM crash is in good agreement with the limit set by finite- $n$  peeling-ballooning instabilities, both at low and high  $\delta$ , across the entire power scan at low gas injection, which results in beta values ranging from  $\beta_N \sim 1.5$  to  $\beta_N \sim 3$  [17]. This is illustrated in Figure 5, where the experimental total pedestal top pressure is compared for each point of the power/ $\beta_N$  scan to the corresponding predicted pedestal top pressure at the P-B boundary, showing good agreement. The higher pedestal pressure obtained at high beta with the high  $\delta$  shape is also consistent with the model predictions. In particular, increasing core pressure stabilizes the ballooning modes due to the increased Shafranov shift, thereby raising the P-B boundary (see also ref. [17] for further details). In summary, we find that the pedestal stability of JET-ILW H-modes at low  $D_2$  gas injection is consistent with the P-B model, both at low and high  $\delta$  and both at low and high  $\beta_N$ .

We note, however, that the minimal  $D_2$  gas injection rates used for these power scans, although entirely suitable for comparative confinement studies of JET-ILW and JET-C H-modes [13], are not always compatible with stable ELMy H-mode plasma conditions over longer time scales, which require integration of the constraints imposed by operation with the W divertor [18]. Higher  $D_2$  gas injection levels are typically needed to maintain low enough divertor target temperatures to reduce W sputtering and therefore control W influxes through the pedestal into the core plasma. In addition, increasing  $D_2$  gas injection increases the ELM

frequency, thus facilitating W flushing by ELMs. The combination of these two effects allows stable ELMy H-mode operation with the ITER-like wall. In this work a stable discharge is defined as having main plasma parameters constant within 10% of their ELM-averaged values over at least  $4 \times \tau_E$ , typically throughout the entire  $I_p$  flat-top and main heating phase ( $\sim 10 \times \tau_E$  or longer).

The power scan at low  $\delta$  was thus repeated at higher  $D_2$  gas injection rates, typical of JET-ILW steady H-mode conditions, to provide a connection with the ELMy H-mode operational space at higher  $I_p/B_t$  and to enable a systematic study of the separate effects of beta and gas injection (or neutral content in the plasma) on pedestal confinement and stability. These experiments are discussed in the next Section.

## 4. Effect of neutrals

### 4.1. Power and $D_2$ gas scans

The low  $\delta$  power scan at low gas injection was repeated at two, higher  $D_2$  gas injection rates, roughly doubling the average gas rate from one power scan to the next, from 2.8 to 8.4 to  $18 \times 10^{21}$  e/s. The maximum achieved  $\beta_N$  – at similar  $P_{sep} \sim 13$  MW (where  $P_{sep}$  is the net power across the separatrix,  $P_{sep} = P_{heat} - dW/dt - P_{rad,bulk}$ ) – decreases with increasing  $D_2$  gas rate, from 2.75 down to 1.95, as shown in Figure 6a. Nonetheless, all discharges are found to be in the type I ELMy H-mode regime, according to the usual definition of ELM frequency,  $f_{ELM}$ , increasing with  $P_{sep}$  [19] as shown in Figure 6b. Figure 6b also shows that the three power scans belong to three separate branches with respect to beta and ELM frequency, both in terms of their absolute values and in terms of their rate of increase with  $P_{sep}$ . In particular, in the plasmas with low  $D_2$  injection rate the ELM frequency remains low and increases much more weakly with power than in the plasmas with highest  $D_2$  rate. Figure 7 shows that also the inter-ELM evolution of these plasmas are qualitatively very different between the power scan at lowest and highest  $D_2$  rate, as illustrated by the time traces of the inner and outer divertor BeII and  $D\alpha$  photon fluxes.

Pedestal top temperatures and densities are derived from *mtanh* fits of ELM-averaged composite profiles of HRTS and ECE data for  $T_e$  and HRTS and Li-beam data for  $n_e$  for the three power scans. Figure 6c shows the variation of  $p_{e,PED}$  vs  $P_{sep}$  as the gas injection rate is increased in the three power scans. At all power levels the pedestal pressure is reduced with high gas injection compared to cases with low gas injection. On average  $n_{e,PED}$  is largely insensitive to the increase in  $D_2$  gas rate and also decreases weakly with increasing input



power. On the other hand,  $T_{e,PED}$  is mostly affected by the increase in gas injection, on average decreasing by a factor of two as the  $D_2$  gas rate increases from lowest to highest and it increases with power for a given  $D_2$  gas rate. Therefore the strong variation in pedestal collisionality obtained in the power and gas scan experiments at low  $\delta$  (Figure 6d) is mainly driven by the variation in pedestal top temperature, while the variations in  $n_{e,PED}$  and  $Z_{eff}$  contribute more weakly to it. As expected, the variations in  $v_{e,PED}^*$  and  $\beta_{pol,PED}$  are correlated in these experiments.

Analysis of the pre-ELM pedestal structure indicates that the electron pressure width in psi space widens with increasing  $D_2$  gas rate, as shown in Figure 8a and 8b. To try and reduce scatter in the data,  $\Delta_{pe}$  is normalized to  $(\beta_{pol,PED})^{0.5}$ , under the assumption that the EPED width scaling holds for JET-ILW pedestals, as could be indicated by the data of Figure 4. It is interesting to note that with this normalization also the pedestal pressure widths of the high  $\delta$  power scans at low gas rate fall in line with the trend of  $\Delta_{pe}$  increasing with  $D_2$  gas level. On the other hand,  $\Delta_{pe}/(\beta_{pol,PED})^{0.5}$  shows no appreciable variation with  $v_{e,PED}^*$ . The pressure gradient increases with  $\beta_{pol,PED}$  at low  $D_2$  gas rate, as discussed in section 3, whereas at medium to high gas rate it remains constant. Therefore the weaker increase in  $p_{e,PED}$  at medium/high  $D_2$  gas rates is due to broadening of the pedestal width at constant gradient.

The evolution of the pedestal structure in the power and gas scans, discussed above, exhibits similarities with the measurements obtained in  $D_2$  gas scans at constant input power in 2.5MA/2.7T high  $\delta$  ELMy H-modes, analyzed in detail in [20]. In those experiments, with increasing  $D_2$  gas rate the pressure gradient decreases and the width increases at constant  $\beta_{pol,PED}$  [20]. In particular, the increase in  $D_2$  gas rate at constant input power results in the increase in  $v_{e,PED}^*$  at constant  $\beta_{pol,PED}$ . These observations challenge the EPED model predictions, as the pedestal widens at constant  $\beta_{pol,PED}$  but with increasing  $v_{e,PED}^*$  ( $D_2$  gas rate), thus deviating from the KBM-based dependence of the pedestal width with  $\sqrt{\beta_{pol,PED}}$ .

These observations may indicate an additional dependence of the pedestal pressure width on other parameters than only  $\beta_{pol,PED}$ , either directly or indirectly connected with D neutral penetration in the pedestal region.

## 4.2. Edge stability analysis

In order to assess the effect of increased neutral content in the plasma on the pedestal stability, ELITE numerical runs were carried out at the lowest and highest  $\beta_N$  range of the

power scans at the three D<sub>2</sub> gas injection rates. The results are summarized in Figure 9a. Here the same representation of Figure 5 is used, namely solid symbols for the experimental total pedestal top pressure and open symbols for the calculated pressure at the P-B stability boundary. In this representation, the distance of the operational point to the P-B boundary is given by the length of the green arrow for the data point at  $\beta_N \sim 2$  (JET pulse #87341, gas rate =  $8.4 \times 10^{21}$  e/s). Figure 9b exemplifies the same case in the  $j_{\text{edge}}-\alpha_{\text{max}}$  diagram, where the operational point is represented by the green star and the distance to the P-B boundary – illustrated by the green dashed arrow – is calculated self-consistently at fixed pedestal width and increasing  $T_{e,\text{PED}}$ . The stability calculations were carried out for toroidal mode numbers up to  $n = 50$  (see e.g. Figure 9b) and using  $\gamma > 0.03 \times \omega_A$  as stability criterion (with  $\gamma$  the growth rate and  $\omega_A$  the Alfvén frequency), as previously done for stability analysis of JET-C pedestals [21]. Accordingly, at low gas rate (blue circles in Figure 9a) the pedestals are found near the P-B stability boundary before the ELM crash, both at high and low beta as discussed in Section 3 (see Figure 4). In contrast, at intermediate and high D<sub>2</sub> gas rates (green and magenta symbols in Figure 9a) the type I ELMy H-mode pedestals are found to be deeply stable to intermediate- $n$  P-B instabilities at higher  $\beta_N$ . Thus, the weaker increase in pedestal pressure with power observed at high D<sub>2</sub> gas rates does not appear to be consistent with the P-B model, at least in the ELITE calculations run with the assumptions described above. As these type I ELMy pedestals are characterized by low edge current and high collisionality, and thus populate the ballooning region of the stability diagram, possible sources of discrepancy between experiment and P-B model could be connected with the model used for the calculation of the bootstrap current and/or with larger uncertainties in the definition of the stability boundary for pure high- $n$  ballooning modes. In the following sections we address these issues separately.

#### 4.2.1. Impact of bootstrap current models on the edge stability results

One possible source for the discrepancy between the results of the ELITE stability analysis and the experimental data may be connected with the calculation of the edge bootstrap current in conditions of high collisionality, achieved in our case at high D<sub>2</sub> gas injection. A recent comparison between simulation results with the drift kinetic code NEO [22], [23] and the Sauter model [16] for low and high collisionality DIII-D discharges has shown the Sauter model to overestimate  $j_{\text{BS}}$  at high collisionality and to underestimate it at low collisionality [24]. This work thus motivated comparison of the two bootstrap current models for the experimental conditions of the JET-ILW pedestals of the power and gas scans.

For the NEO runs we have assumed equal electron and ion temperatures, constant line averaged  $Z_{\text{eff}}$ , a single impurity species (= Be) and local, no orbit effects. Starting from the experimental profiles, the sensitivity of the two  $j_{\text{BS}}$  models to variations in collisionality and in  $Z_{\text{eff}}$  have been investigated by means of temperature and  $Z_{\text{eff}}$  scans, respectively. It is found that in order to test the accuracy of the Sauter model a good figure of merit is the value of  $\nu^*$  at the peak of the pedestal current. The key results of the analysis can be summarized as follows: i) at low collisionality ( $\nu^* < 1$ ) and  $Z_{\text{eff}} \sim 1$ , the Sauter and NEO models agree very well; ii) at high collisionality ( $\nu^* > 1$ ) and  $Z_{\text{eff}} \sim 1$ , the Sauter model overestimates  $j_{\text{BS}}$ , relative to NEO, in agreement with the results of [24]; iii) for  $Z_{\text{eff}} \gg 1$  an additional, competing effect is found, which causes the Sauter model to underestimate  $j_{\text{BS}}$  relative NEO: at  $\nu^* > 1$  this effect can compensate the overestimate of Sauter w.r.t. NEO, leading to very similar  $j_{\text{BS}}$  values in the two cases, while at very low collisionality (so far, usually found radially inwards of the peak of  $j_{\text{BS}}$ ) it will always cause the Sauter model to underestimate  $j_{\text{BS}}$ . Figure 10 shows the two extreme examples of this case study: Figure 10a compares the edge bootstrap current profiles calculated with Sauter's formula and with NEO for a JET-ILW pedestal at low collisionality (low gas, high power pulse #84794) while Figure 10b shows the comparison for the pedestal at highest collisionality and lowest  $j_{\text{BS}}$  in the scan (high gas, low power shot #87346). The two calculations agree well at low collisionality, except near the separatrix, whereas at high collisionality the Sauter calculation overestimates that from NEO by almost 100%.

Comparative ELITE runs with  $j_{\text{BS}}$  calculated according to Sauter's formula (in red) and NEO (in blue) are shown in Figure 11 for the pedestal at low (low gas/high power, #84794) and highest collisionality (high gas/low power, #87346) of the power and gas scans. The ELITE calculations were run with  $n_{\text{max}} = 70$  and  $\gamma > 0.03$   $\omega_A$  was used to define the stability criterion. At low collisionality (Figure 11a) the two bootstrap current models give identical results (not distinguishable in the figure). On the other hand, in the high collisionality case the choice of  $j_{\text{BS}}$  model influences the edge stability: the NEO calculations drive the operational point to lower maximum edge current and also modify the peeling boundary (Figure 11b). However, in both cases the operational point is close to the ballooning boundary within  $\sim 15\%$  and the overall difference between the two stability analyses is certainly not larger than the uncertainties in the experimentally measured pressure gradient and definitely smaller than other uncertainties associated with the stability analysis procedure, as discussed in the following sections. The peeling boundary changes more with the choice of

the bootstrap current model. This is due to changes in the shape of the current profile, as shown in Figure 10b. Compared to NEO, Sauter's formula gives higher current at the foot of the pedestal near the separatrix, which is destabilising for the peeling modes, therefore reducing the peeling boundary [25]. However, this modification does not affect the result of the stability analysis of the cold, high  $v^*$  pedestal of pulse #87346, which is limited by high- $n$  ballooning modes.

Of all pedestals of the JET-ILW low  $I_p$ , power and gas scans, the one of pulse #87346 is that where we find the largest reduction in edge bootstrap current with NEO compared to the Sauter formula. Therefore, from this sensitivity study we conclude that a more accurate calculation of  $j_{BS}$  in conditions of high pedestal collisionality does not fully account for the discrepancy between operational point and P-B model predictions of the ELM onset concerning the weaker increase of pedestal pressure with beta at high  $D_2$  gas rates in JET-ILW.

#### 4.2.2. Impact of stability criteria on the shape of the stability boundary

In the stability diagrams of Figures 11a and 11b,  $\gamma > 0.03 \omega_A$  defines the stability criterion (as e.g. in the diagram of Figure 9b). However, the choice of stability criterion is somewhat arbitrary and  $\gamma > c \omega_{*max}^*$  is also often used in the literature [7], with  $c$  a constant  $< 1$ . As  $\omega_{*max}^*$  is proportional to the pressure gradient and varies strongly in the pedestal, which value to use for  $c$  is also a matter of debate. For this investigation we select  $c = 0.25$ . The choice of stability criterion can have a larger impact on the ELITE calculations of the pedestals under study, as shown in Figures 12a and 12b. In the low collisionality case (#84794, Figure 12a), where the Sauter and NEO  $j_{BS}$  calculations are in agreement, no difference is found in the operational point (red star coinciding with blue star), the peeling boundary is slightly affected, but the ballooning boundary expands when  $\gamma > 0.25 \omega_{*max}^*$  is chosen (blue dashed line). However, as the instabilities limiting the pressure gradient are intermediate- $n$  P-B modes, the result of the stability analysis is hardly influenced by which stability criterion is used. In the high collisionality case (#87346, Figure 12b) the pure low- $n$  peeling mode becomes relevant with  $\gamma > 0.25 \omega_{*max}^*$  criterion and the operational point is deeply stable in this representation. For comparison, the stability boundary of the most unstable,  $n = \infty$  ballooning mode is also shown (short dashed line).

#### 4.2.3. Effect of maximum $n$ number on the pedestal stability analysis

The edge stability analyses of Figures 11 and 12 were performed extending the ELITE runs to a maximum toroidal mode number  $n_{max} = 70$ , which was needed to address the

pedestal stability of the high collisionality shot #87346. We therefore investigate the effect of varying  $n_{\max}$  in the ELITE calculations, which may be relevant to the edge stability analysis of cold pedestals close to the ballooning boundary. As an example, in Figure 13 we compare for the high collisionality pedestal of shot #87346 and  $j_{BS}$  from NEO the simulations with ELITE run to  $n = 50$  (pink boundaries) and  $n = 70$  (blue boundaries). The stability criterion is  $\gamma > 0.03 \omega_A$ . This sensitivity test indicates that increasing  $n$  from 50 and 70 in ELITE affects the ballooning boundary, as expected (see e.g. [25], [26]), and that the solution with  $n = 70$  is closer to the experiment.

In summary, in JET-ILW operation at high beta and low  $D_2$  gas rates is a necessary condition for good pedestal (and core) performance. In these conditions the pedestals are largely consistent with the P-B paradigm and the EPED model can predict the pedestal height within the usually quoted  $\pm 20\%$  confidence interval. In contrast, the weaker increase in pedestal pressure with power at high  $D_2$  gas rates – necessary for W control, in particular at higher  $I_P/B_T$  - is not consistent with the peeling-ballooning model, even allowing for the large uncertainties associated with the stability analysis of cold pedestals close to the ballooning boundary discussed above. In these conditions, missing physics in the models - possibly linked with neutral penetration setting the pedestal width - may be required to explain the onset of the ELM instability.

### 4.3. Variations in divertor configuration

The 2012 JET-ILW experiments showed that the energy confinement of low  $\delta$  ( $\sim 0.2$ ), low beta ( $\beta_N < 1.5$ ) ELMy H-modes is largely reduced due to the need for higher  $D_2$  gas injection rates than in JET-C, as a measure against high W influxes through the pedestal into the core plasma [1]. These plasmas were run with a divertor configuration with the inner strike point on the Vertical target and the outer strike point on the bulk W, semi-Horizontal target (here denoted as V/H divertor configuration), as illustrated in Figure 14.

New experiments in 2013-2014 aimed at optimizing the confinement of low  $\delta$ , 2.5MA/2.7T ELMy H-modes have shown that when the effective neutral recycling is reduced, e.g. by placing both strike points close to the pumping duct (the so-called ‘Corner’ divertor configuration, C/C, see Figure 14), good confinement,  $H_{98} \sim 1$  at  $\beta_N \sim 2$ , can be recovered in discharges that are steady over the entire additional heating phase ( $> 10 \times \tau_E$ ) [8]. Edge stability analysis with ELITE shows that in such cases the operational point is found at, or even marginally above, the P-B stability boundary.

The increase in total thermal stored energy, observed in the C/C configuration as compared to V/H, is related to an increase in core pressure at otherwise similar pedestal pressures. In particular, operation in C/C configuration, which leads to a 2-3 fold increase in sub-divertor neutral pressure and thus improved cryo-pumping compared to the V/H configuration, allows a decrease in  $n_{e,PED}$  and an increase in  $T_{e,PED}$  (and  $T_{i,PED}$ , as measured by edge charge exchange) at similar  $p_{e,PED}$  values, while simultaneously maintaining W control and thus stable ELMy H-mode conditions. This is illustrated in the edge diagram of Figure 15a (red squares) for a dataset of low  $\delta$ , 2.5MA/2.4-2.7T JET-ILW ELMy H-modes with auxiliary heating powers of 15 - 23 MW, provided by neutral beam injection. Conversely, in the V/H configuration (blue diamonds in Figure 15a), with poorer pumping capability, similar pedestal pressures are achieved, but at lower  $T_{e,PED}$  and higher  $n_{e,PED}$  values, hence typically at higher edge collisionality (see Figure 15b). The lower edge collisionality of ELMy H-modes in C/C configuration is well correlated with an increase in density peaking (Figure 15b), consistent with the work of [27]. More peaked core density profiles and thus higher pressure peaking, while  $T_e$  peaking remains unvaried, leads to an increase in global thermal stored energy in C/C configuration compared to V/H, at otherwise similar  $p_{PED}$  but lower collisionality, as shown by the electron kinetic profiles of Figure 16 [28]. The best performing low  $\delta$ , 2.5MA/2.7T ILW H-modes are those in C/C configuration achieving  $T_{e,PED}$  values of 1-1.2 keV (see Figure 15a, red squares and Figure 1, open red circles), with  $H_{98} \sim 1$  and  $\beta_N \sim 1.8 - 2.0$  [29]. On the other hand, increasing the  $D_2$  gas rate in C/C configuration eventually drives the discharges to conditions of low  $T_{e,PED}$  and higher  $n_{e,PED}$ , similar to those in V/H configuration (red squares underneath blue diamonds in Figure 15a), thus degrading the global energy confinement.

Experiments in 2013-14 have also investigated the effect of varying the inner and/or outer divertor strike point location on pedestal and global confinement. A deleterious effect on  $W_{PED}$  is observed in 2.5MA/2.7T H-modes, at similar input powers and  $D_2$  gas rates as in V/H configuration, when the outer strike point is placed on the outer vertical divertor target and the inner strike point remains in the corner (denoted here C/V divertor configuration and illustrated in green in Figure 14) while maintaining the main plasma shape constant [30]. In the C/V configuration, lower  $n_{e,PED}$  is observed than in V/H, but at similarly low  $T_{e,PED}$  values, as shown by the green circles in Figure 15a. This results in lower  $p_{PED}$  than in the V/H and C/C configurations. Good pumping is achieved in the C/V configuration, possibly also helped by the proximity of the inner strike point to the inner divertor corner participating in

the effective pumping. This is likely to lead to the lower pedestal density observed in this configuration [30]. The average collisionality of the discharges in C/V configuration is intermediate between the higher  $\nu^*$  in the V/H configuration and the lowest  $\nu^*$  achieved in the C/C configuration and no sizeable increase in density peaking is observed (Figure 15 and Figure 16, top right panel). Overall, this leads to low pedestal *and* low core pressure in C/V configuration (Figure 16) and thus to the lowest confinement of the three configurations investigated [28], [30].

Analysis of neutral re-circulation patterns in these experiments indicates that the neutral recycling in the divertor is not correlated with the observed variations in confinement, whereas the neutral pressure in the main chamber varies inversely with the energy confinement [30]. It is plausible that a change in divertor configuration may lead to a change in the leakage of neutrals towards the main chamber, thus affecting the main chamber neutral pressure. The pedestal pressure and the main chamber neutral pressure are found to be anti-correlated: the observed decrease in  $T_{e,PED}$  from C/C configuration to either V/H or C/V configurations appears to be correlated to an increase in main chamber neutral pressure (at fixed input power and  $D_2$  injection rate) as analysed in further detail in [30]. However, it is not possible at present to establish a causal relationship between these observations. These findings are akin to the results of a recent analysis of the loss of confinement in high  $\delta$  hybrid scenario in JET-C, showing a correlation between loss of confinement and increase in the neutral pressure and recycling in the main chamber [31], [13].

The changes in neutrals recirculation patterns induced when varying the divertor configuration are also correlated with differences in the ELM dynamics. For instance, when comparing ELMy H-modes in V/H vs C/C divertor configurations, it is observed that at higher  $T_{e,PED}$  (obtained in C/C configuration) the ELM energy losses, the width of the ELM affected volume and duration of the ELM crash are similar to those observed in JET-C [8]. Conversely, at lower  $T_{e,PED}$  values signatures of inter-ELM detachment are observed at the inner divertor, the MHD ELM crash time is longer in JET-ILW V/H configuration ( $\sim 1-2$  ms) [8], [11], [32] and the recovery of the density pedestal is delayed to 8-10 ms, possibly caused by a transient reduction in the D recycling coefficient after the ELM crash, with the W target plate acting as an additional particle sink compared to case with CFC divertor [33].

2D divertor/SOL modelling of these discharges was carried out in order to investigate the interaction of the D neutrals with the pedestals. Charge exchange losses in the pedestal were found to be negligibly small and thus unlikely to explain the observed reduction in

energy confinement [34], [35], [30]. Therefore, other possible mechanisms are under investigation and further experimental and modelling work is required in order to explain the physics underlying the degradation in confinement in JET-ILW with decreased pumping or increased D<sub>2</sub> gas injection.

#### 4.4. Effect of low Z impurities

The reduction in energy confinement of JET-ILW low beta, high  $\delta$  H-modes can be largely compensated by N<sub>2</sub> seeding: pedestal pressures approaching those of JET-C H-modes can be achieved at the same plasma density and auxiliary heating [2]. In these plasmas the marginal P-B mode stability at the end of the ELM cycle is resumed [26]. Analysis of the pedestal structure shows that the increase in pedestal height is found to be due to broadening of the pedestal pressure width with increasing level of N<sub>2</sub> injection and to an increase in peak pressure gradient up to an optimum value of N<sub>2</sub> seeding rate, after which the peak pressure gradient starts to decrease [20]. In particular, as the N<sub>2</sub> seeding rate is increased in the experiment, the temperature pedestal widens more strongly than the peak temperature gradient decreases, so that overall  $T_{e,PED}$  increases. The peak density gradient increases at constant density pedestal width up to an optimum value of N<sub>2</sub> seeding rate, thus leading first to an increase and then to a decrease in  $n_{e,PED}$ . The overall effect is thus an increase in  $p_{e,PED}$  up to N<sub>2</sub> seeding rates of  $\sim 1.5 \times 10^{22}$  e/s, followed by constant  $p_{e,PED}$  as the N<sub>2</sub> rate is increased further to  $\sim 2.5 \times 10^{22}$  e/s [20]. The corresponding increase in line averaged  $Z_{eff}$  is from  $\sim 1.2$ - $1.3$  without N<sub>2</sub> seeding (with Be being the main intrinsic impurity) to  $\sim 1.8$  at the highest N<sub>2</sub> seeding levels for the 2.6T/2.5MA dataset [2]. These values are to be compared with  $Z_{eff} \sim 2.0$ - $2.5$  in the corresponding JET-C high  $\delta$  dataset (where C was the dominant intrinsic impurity). The uncertainty in the  $Z_{eff}$  measurements is of order 20%. Further experiments in 2013-14 have shown that the magnitude of the increase in pedestal pressure with N<sub>2</sub> seeding in JET-ILW depends on plasma triangularity, the increase being larger in high  $\delta$  (40%) than in low  $\delta$  plasmas (15%) [26]. In high  $\delta$  ELMy H-modes with both strike points on the vertical targets (V/V) similar results are observed in terms of  $T_{e,PED}$  variations with N<sub>2</sub> injection rate – indicating that this result is independent of divertor configuration - while  $n_{e,PED}$  decreases with increasing N<sub>2</sub> seeding rate [26], in agreement with EDGE2D/EIRENE modelling results [32].



The physics underlying the observed increase in  $T_{e,PED}$  with  $N_2$  seeding is not yet understood and is a subject of on-going work, both experimentally and on the modelling side. The increase in ion dilution with  $N_2$  seeding, which lowers the total pressure gradient and thus allows higher  $T_{e,PED}$  to be achieved, is not sufficient to explain the full magnitude of the  $T_{e,PED}$  increase observed in the experiment.

Further experiments and modelling are planned, both in JET-ILW and in other tokamaks, in order to understand the effects of low- $Z$  impurities on pedestal confinement and stability and to optimize the impurity combination for each device. This will provide key input for predictive models of the pedestal height, in particular in view of predicting ITER's performance. Based on the JET-ILW results, it is plausible that current pedestal models need to be refined, by including the role of scrape-off-layer physics, low- $Z$  impurities and neutral recycling. On the experimental side, work is in progress for the derivation of  $Z_{eff}$  profiles in JET-ILW, so as to quantify the local changes of low- $Z$  impurity concentrations in the edge plasma and their impact on the pedestal structure. The approach followed here is that of forward modelling of the continuum emission from multiple spectroscopic diagnostics (sampling different spectral and radial regions of the plasma) using Bayesian methods. An edge peaked  $Z_{eff}$  profile would increase the EPED predicted  $T_{e,PED}$  as seen in the experiment.

## 5. Conclusions

H-mode experiments in JET with an ITER-like Be/W wall have challenged our current understanding of pedestal stability. On one hand the P-B paradigm describes well the JET-ILW pedestals at low gas injection (low neutral content in the plasma), both at low and high beta. On the other hand, high delta pedestals at high  $D_2$  injection rates are not consistent with EPED model predictions, as the pedestal widens at constant  $\beta_{pol,PED}$  but with increasing  $v_{e,PED}^*$  and thus the experiment deviates from the KBM-based dependence of the pedestal width with  $\sqrt{\beta_{pol,PED}}$  [20]. These results may indicate an additional dependence of the pedestal pressure width on other parameters, either directly or indirectly connected with the D neutral content in the plasma. The JET-ILW power scans at different  $D_2$  gas injection rates (i.e. with varying neutral content in the plasma) indicate that the role of neutrals on pedestal stability should be addressed. Alternatively, it may be that the ELMs we observe in conditions of high neutral content, despite being of type I, are of resistive nature - e.g. more similar to type III ELMs - and therefore not described by the P-B paradigm. In these experiments the pedestal pressure width normalized to  $\sqrt{\beta_{pol,PED}}$  does not vary with

$v_{e,PED}^*$  but is systematically wider at higher than at lower  $D_2$  gas rates. This may imply that atomic physics effects could also contribute in setting the pedestal width. In some cases low beta, high  $\delta$  plasmas are detached on the inner divertor leg and thus have a cold and dense X-point. This could affect the upstream kinetic profiles in the pedestal gradient region, thus the impact of changes in divertor/SOL conditions on pedestal stability should be investigated. The drastic reduction in C concentration from JET-C to JET-ILW and the effect of  $N_2$  seeding on pedestal confinement point to the necessity of taking a closer look at the effect of low-Z impurities on pedestal stability. In particular, we need to understand what physics mechanisms lead, with  $N_2$  seeding, to an increase in  $T_{e,PED}$  in high  $\delta$  plasmas in JET-ILW, while replacing C with Be is associated with a decrease in  $T_{e,PED}$ . As JET pedestals do not appear to be KBM-limited [36], we also need to think of how we can resolve the pedestal structure and its evolution. Global gyrokinetics and/or nonlinear GK should be considered as possible next steps in pedestal models. Alternatively, another paradigm may be needed, which does not invoke pedestal height limited by KBMs. Ultimately, future pedestal modelling should also address isotope effects, self-consistency between core and edge, effect of fast ions, difference in temperature and density profile structure, to name a few aspects that need to be considered in order to progress towards full predictive capability of the pedestal height.

### Acknowledgements

This work has been carried out within the framework of the EUROfusion Consortium and has received funding from the EURATOM research and training programme 2014-2018 under grant agreement No 633053. The views and opinions expressed herein do not necessarily reflect those of the European Commission.

### References

- [1] BEURSKENS, M., et al., Plasma Phys. Control. Fusion **55** (2013) 124043.
- [2] GIROUD, C., et al., Nucl. Fusion **53** (2013) 113025.
- [3] SAARELMA, S., et al., 14th H-mode workshop 2014.
- [4] WILSON, H. R., et al., Phys. Plasmas **9** (2002) 1277 and SNYDER, P., Phys. Plasmas 2002.
- [5] SNYDER, P., Phys. Plasmas **16** (2009) 056118.
- [6] SNYDER, P.B., et al., Nucl. Fusion **51** (2011) 103016.
- [7] SNYDER P.B., et al., Nucl. Fusion **44** (2004) 320.

- [8] DE LA LUNA, E., et al., ‘*Comparative study of high triangularity H-mode plasma performance in JET with Be/W and CFC wall*’, 25<sup>th</sup> IAEA FEC Conference, St Petersburg, Russian Federation, 2014, EX/P5-29.
- [9] SAIBENE, G., et al., Plasma Phys. Control. Fusion **44** (2002) 1769.
- [10] LEYLAND, M., et al., Nucl. Fusion **53** (2013) 083028.
- [11] BEURSKENS, M., et al., Nucl. Fusion **54** (2014) 043001.
- [12] MAGGI, C.F., et al., Nucl. Fusion **54** (2014) 023007.
- [13] CHALLIS, C.D., et al., Nucl. Fusion **55** (2015) 053031.
- [14] GROEBNER, R.G., et al., Phys. Plasmas **5** (1998) 1800.
- [15] FRASSINETTI, L., et al., Rev. Sci. Instrum. **83** (2012) 013506.
- [16] SAUTER, O. et al., Phys. Plasmas **6** (1999) 2835 & Phys. Plasmas **9** (2002) 5140.
- [17] SAARELMA, S., et al., ‘*The effects of impurities and core pressure on pedestal stability in the Joint European Torus (JET)*’, Phys. Plasmas 2015, accepted.
- [18] NEU, R., et al., Phys. Plasmas **20** (2013) 056111.
- [19] ZOHM, H., et al., Plasma Phys. Control. Fusion **38** (1996) 105
- [20] LEYLAND, M., et al., Nucl. Fusion **55** (2015) 013019.
- [21] SAARELMA, S., et al., Plasma Phys. Control. Fusion **51** (2009) 035001.
- [22] BELLI, E., and CANDY, J., Plasma Phys. Control. Fusion **50** (2008) 095010.
- [23] BELLI, E., and CANDY, J., Plasma Phys. Control. Fusion **54** (2012) 015015.
- [24] BELLI, E. A. et al., Plasma Phys. Control. Fusion **56** (2014) 045006.
- [25] MAGET, P., et al., Nucl. Fusion **53** (2013) 093011.
- [26] GIROUD, C., et al., Plasma Phys. Control. Fusion **57** (2015) 035004.
- [27] ANGIONI, C., et al., Nucl Fusion **47** (2007) 1326.
- [28] FRASSINETTI, L., et al., ‘*Effect of the divertor geometry on pedestal confinement in JET-ILW*’, 41<sup>st</sup> EPS Conference on Plasma Physics, Berlin 2014, P1-030.
- [29] NUNES, I., et al., ‘*Compatibility of high performance operation with JET-ILW*’, 25<sup>th</sup> IAEA FEC Conference, St Petersburg, Russian Federation, 2014, EX/9-2.
- [30] JOFFRIN, E., et al., ‘*Impact of divertor geometry on ITER scenarios performance in the JET metallic wall*’, 25<sup>th</sup> IAEA FEC Conference, St Petersburg, Russian Federation, 2014, EX/P5-40.
- [31] JOFFRIN, E., et al., 41<sup>st</sup> EPS Conference on Plasma Physics, Berlin 2014, O4.125.
- [32] FRASSINETTI, L., et al., Nucl Fusion **55** (2015) 023007.
- [33] BREZINSEK, S., et al., J. Nucl. Mater., in press, doi : 10.1016/j.jnucmat.2014.12.007)

[34] TAMAIN, P., et al., 21<sup>st</sup> International Conference on Plasma Surface Interactions, Kanazawa, Japan, 2014, O33.

[35] JARVINEN, A., et al., '*Comparison of H-mode plasmas in JET-ILW and JET-C with and without nitrogen seeding*', 25<sup>th</sup> IAEA FEC Conference, St Petersburg, Russian Federation, 2014, TH/P5-34.

[36] SAARELMA, S., et al., Nucl. Fusion **53** (2013) 123012.

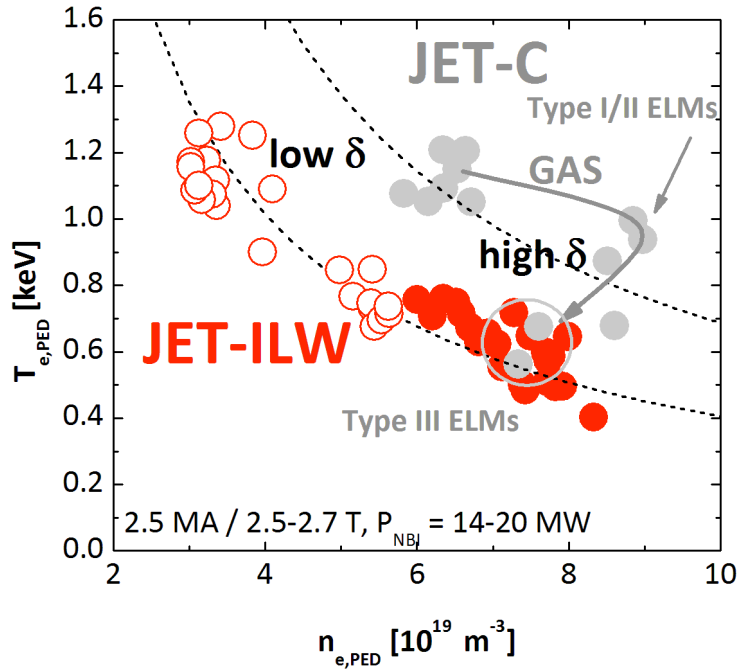


**FIGURE 1.**  $T_{e,\text{PED}} - n_{e,\text{PED}}$  diagram of JET-ILW type I ELMy H-mode dataset at 2.5 MA/2.5-2.7 T,  $P_{\text{NBI}} = 14\text{-}20$  MW,  $\beta_{\text{N}} \sim 1.5$ , from the 2013-2014 experiments in red. Open and solid circles are for the low ( $\sim 0.2$ ) and high ( $\sim 0.4$ )  $\delta$  discharges, respectively, for which similar  $p_{e,\text{PED}}$  are measured. Comparison with data from a gas scan in JET-C (in grey) at similar input parameters shows that the JET-ILW high  $\delta$  type I ELMy H-modes occur in conditions typical of type III ELMy H-modes in JET-C. Data are from the high resolution Thomson scattering diagnostic.

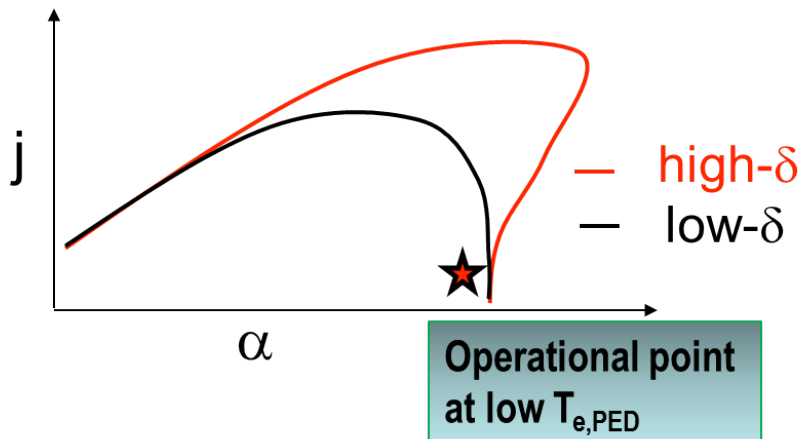


**FIGURE 2.** Cartoon of a  $j - \alpha$  stability diagram, illustrating an operational point at low  $T_{e,\text{PED}}$  - high  $v_{e,\text{PED}}^*$  and low bootstrap current (red star) and the stability boundaries for low (black) and high (red) plasma shape. Increasing  $\delta$  at high  $v_{e,\text{PED}}^*$  does not raise the pedestal height. This is the likely situation for JET-ILW low beta/high collisionality type I ELMy H-modes, where similar pedestal pressures are found at low and high  $\delta$ .

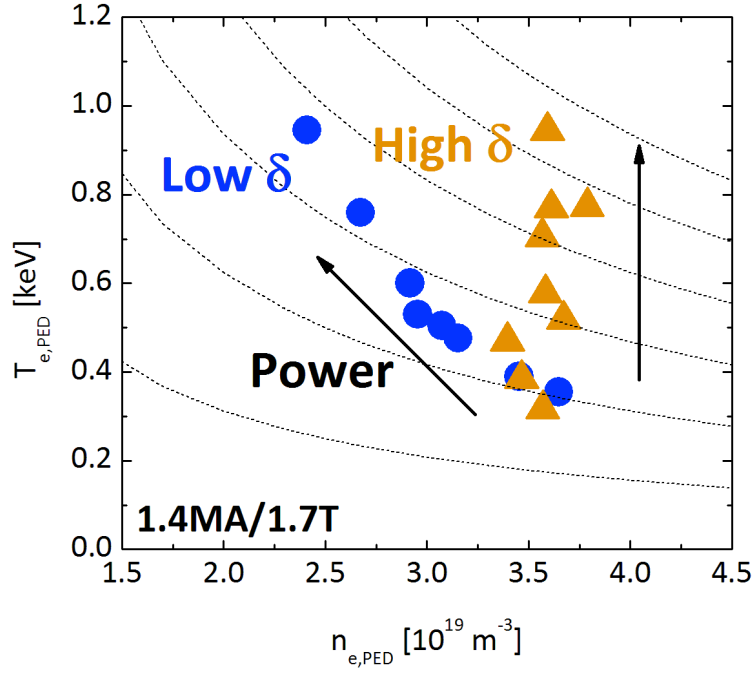


**FIGURE 3.**  $T_{e,PED} - n_{e,PED}$  diagram for the 1.4 MA/1.7 T JET-ILW power scans at low gas injection ( $\Gamma_D \sim 3 \times 10^{21}$  e/s) at low (orange) and high (blue)  $\delta$ , for (V/H) divertor configuration in MkII-HD divertor geometry. High and low  $\delta$  plasmas have similar pedestal pressure at low power/beta. High  $\delta$  plasmas (orange triangles) have higher electron pressure than the low  $\delta$  (blue circles) H-modes at high power/beta. Data are from composite HRTS profiles in the last 30% of the ELM cycle.

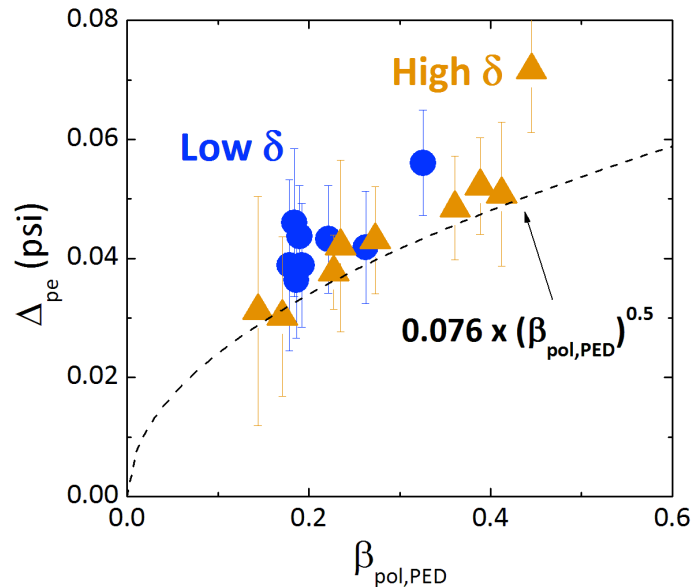


**FIGURE 4.** Electron pedestal pressure width in psi space vs pedestal poloidal beta for the low and high  $\delta$  power scans of Figure 3 compared to the KBM-based pedestal width scaling of  $0.076 \times \beta_{pol,PED}$  in the EPED model.

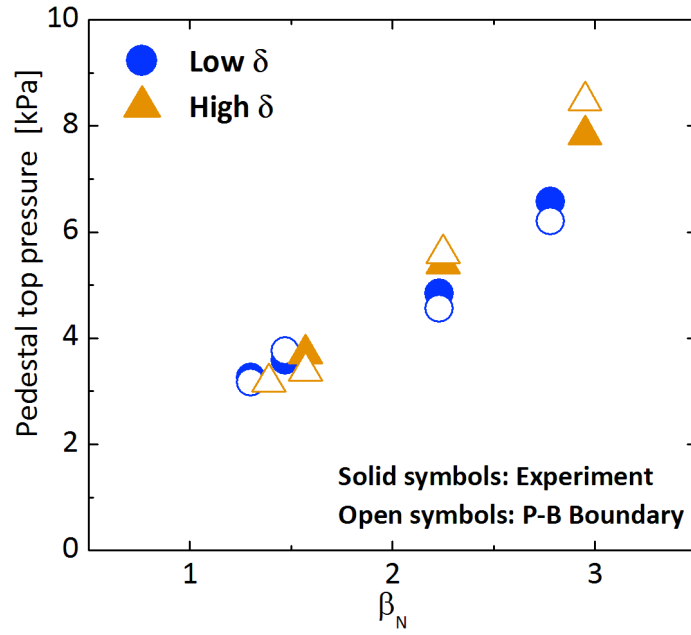


**FIGURE 5.** Comparison of total pedestal top pressure from experiment (solid symbols) and P-B boundary for type I ELM crash, as calculated by HELENA/ELITE (open symbols), versus  $\beta_N$  for the low and high  $\delta$  power scans at low gas injection of Figure 3.

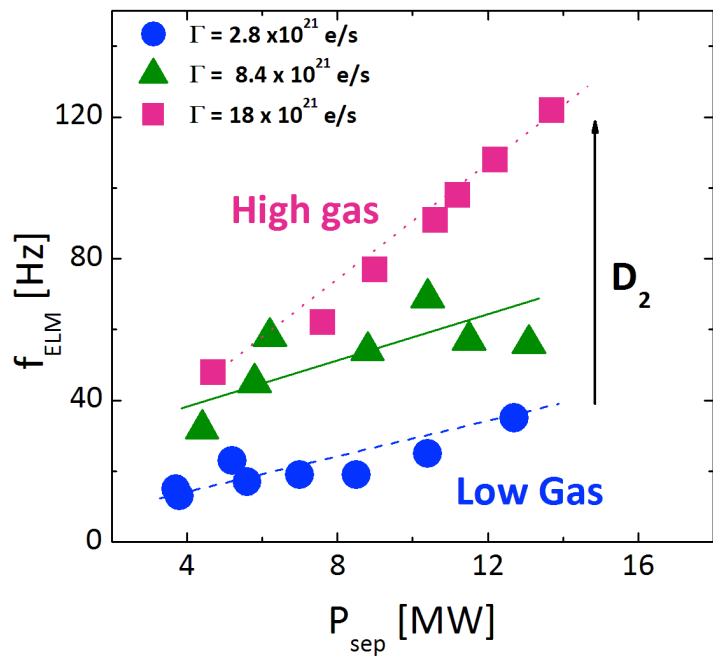
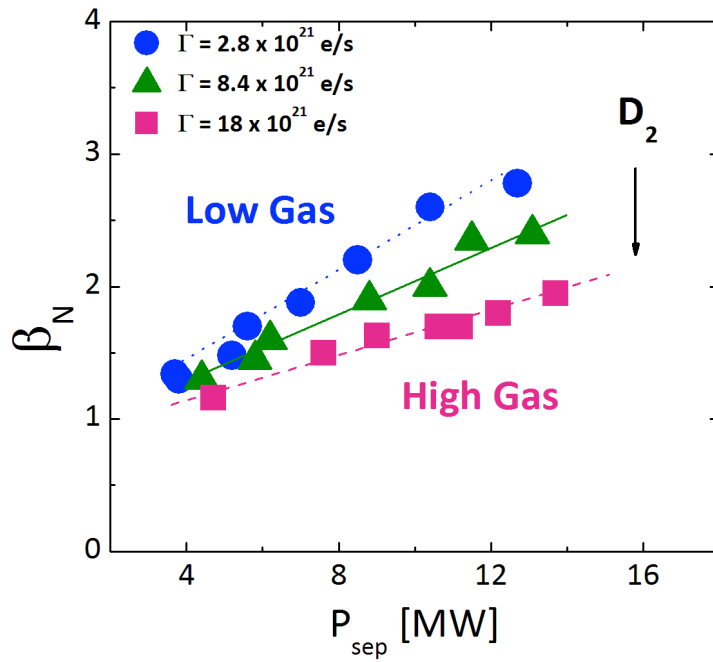
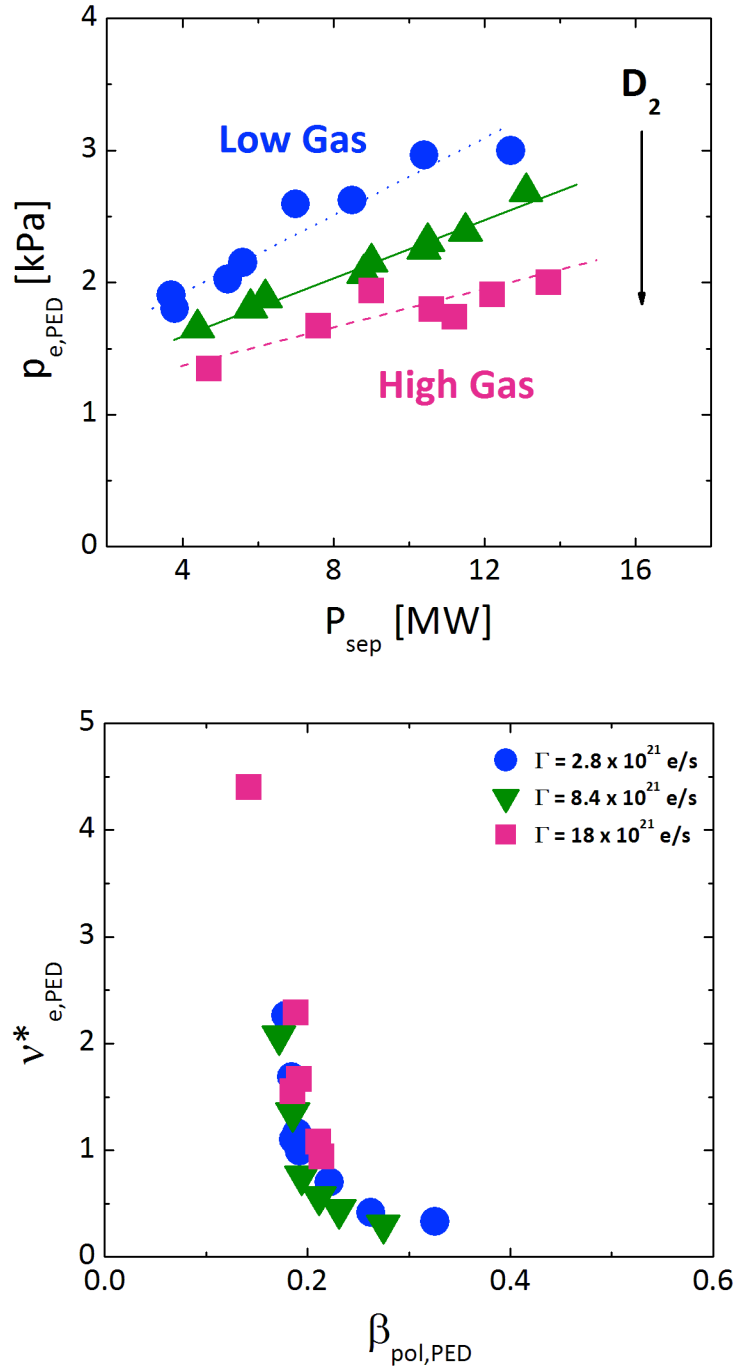
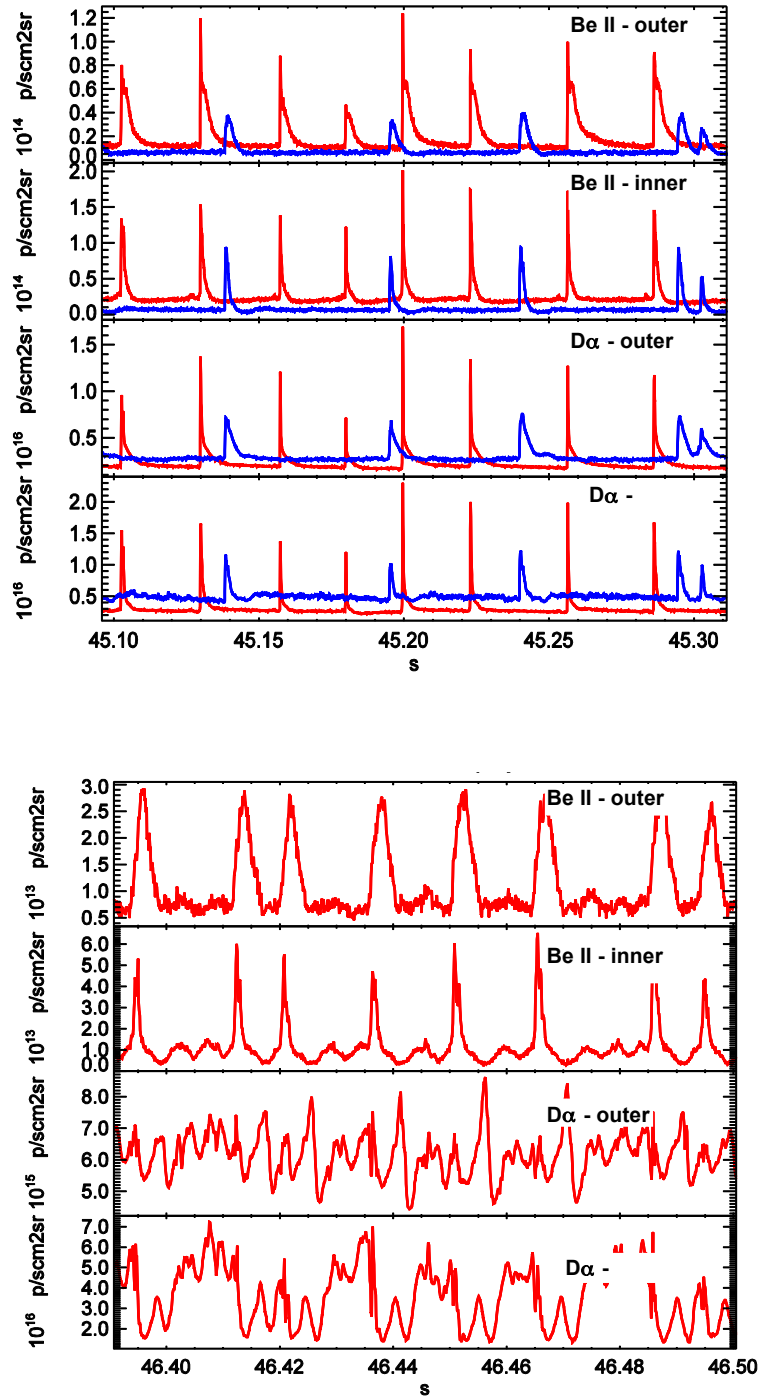


FIGURE 6. / a,b, [caption in next page] ...





**FIGURE 6.** Total normalized beta (a), ELM frequency (b), and ELM-averaged electron pedestal pressure (c) vs  $P_{sep} = P_{heat} - dW/dt - P_{rad,bulk}$  for the three power scans at 1.7T/1.4MA at low  $\delta$ , with increasing levels of  $D_2$  gas injection. All discharges are in the type I ELMy regime. (d): pedestal top collisionality and poloidal beta ranges obtained in the same experiments (pre-ELM values, from HRTS only).



**FIGURE 7.** Outer and inner divertor Be II (527 nm) photon fluxes (top two panels), used as ELM markers in JET-ILW, and evolution of D $\alpha$  photon fluxes during the corresponding ELM cycles (bottom two panels). **(a):** ELM signatures from the power scan at low gas injection, at lowest (blue, #84793) and highest (red, # 84794)  $\beta_N$  in the scan. **(b):** ELM signatures and D $\alpha$  fluxes for discharge #87344 with high gas injection ( $\beta_N = 1.63$ ,  $f_{\text{ELM}} = 77$  Hz). All three H-modes are type I ELMs, as shown in FIGURE 6b.

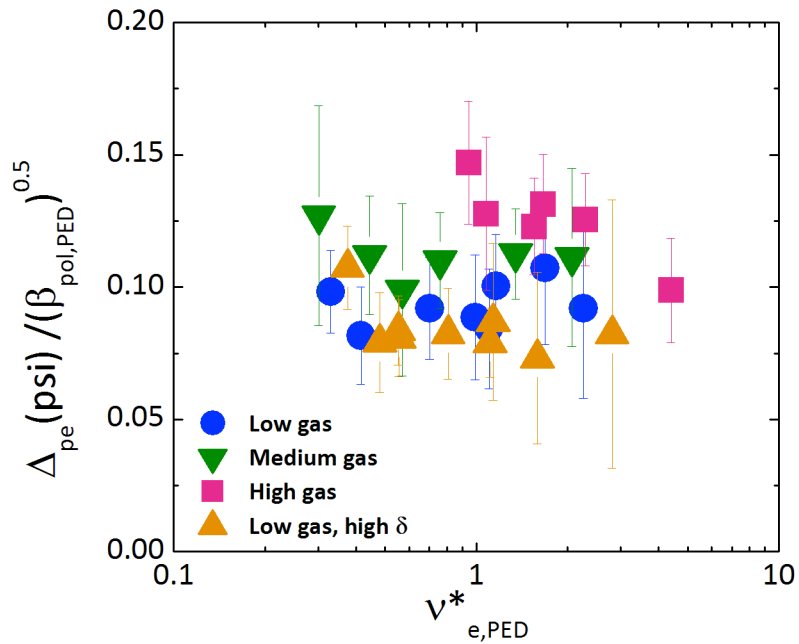
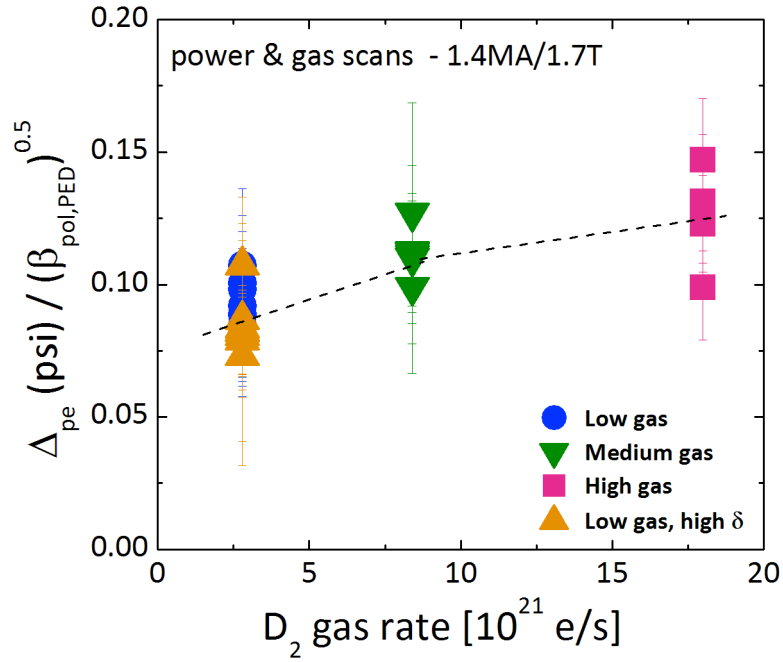


**FIGURE 8.** (a) Pedestal electron pressure width in psi space, normalized to  $\sqrt{\beta_{\text{pol, PED}}}$  vs  $D_2$  gas rate for the power & gas scans at low  $\delta$  and for the low gas power scan at high  $\delta$ ; (b) normalized pedestal electron pressure width vs pedestal top collisionality. All data are from the last 30% of the ELM cycle.

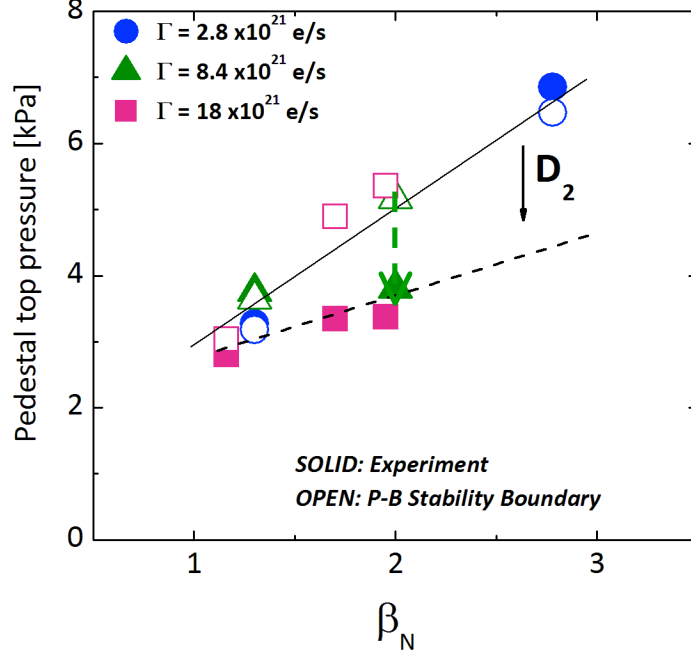


**FIGURE. 9a.** Comparison of P-B stability limit (open symbols) and experimental point (solid symbols) at low (blue), intermediate (green) and high (magenta)  $D_2$  gas rates as a function of  $\beta_N$  for a subset of discharges of the low  $\delta$  power and gas scans of Figure 5. The distance of the operational point to the P-B boundary is indicated by the green arrow, calculated self-consistently with ELITE at fixed pedestal width and increasing  $T_{e,PED}$ . Figure 9b exemplifies in 2D in the corresponding  $j$ - $\alpha$  diagram.

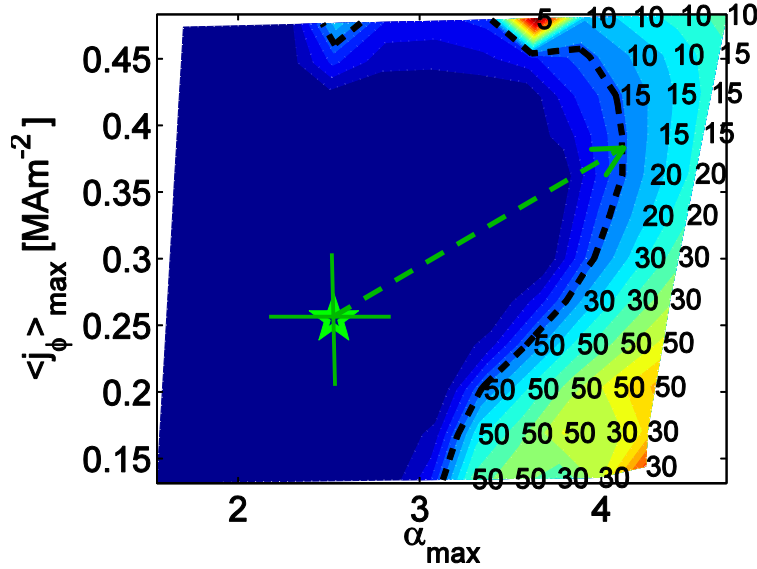


**FIGURE. 9b.**  $j$ - $\alpha$  stability diagram illustrating the distance of the operational point (green star) from the P-B boundary - represented by the length of the green arrow -, as calculated with HELENA/ELITE at fixed pedestal width and increasing  $T_{e,PED}$ , with  $n_{max} = 50$  and  $\gamma > 0.03 \times \omega_A$  as stability criterion. The case is for pulse #87341,  $P_{sep} = 10.4$  MW ( $\beta_N = 2$ ),  $\Gamma_D = 8.4 \times 10^{21}$  e/s. In Figure 9a, the operational point corresponds to the green solid triangle and its distance from the stability boundary (open green triangle) is indicated by the green, broken arrow.

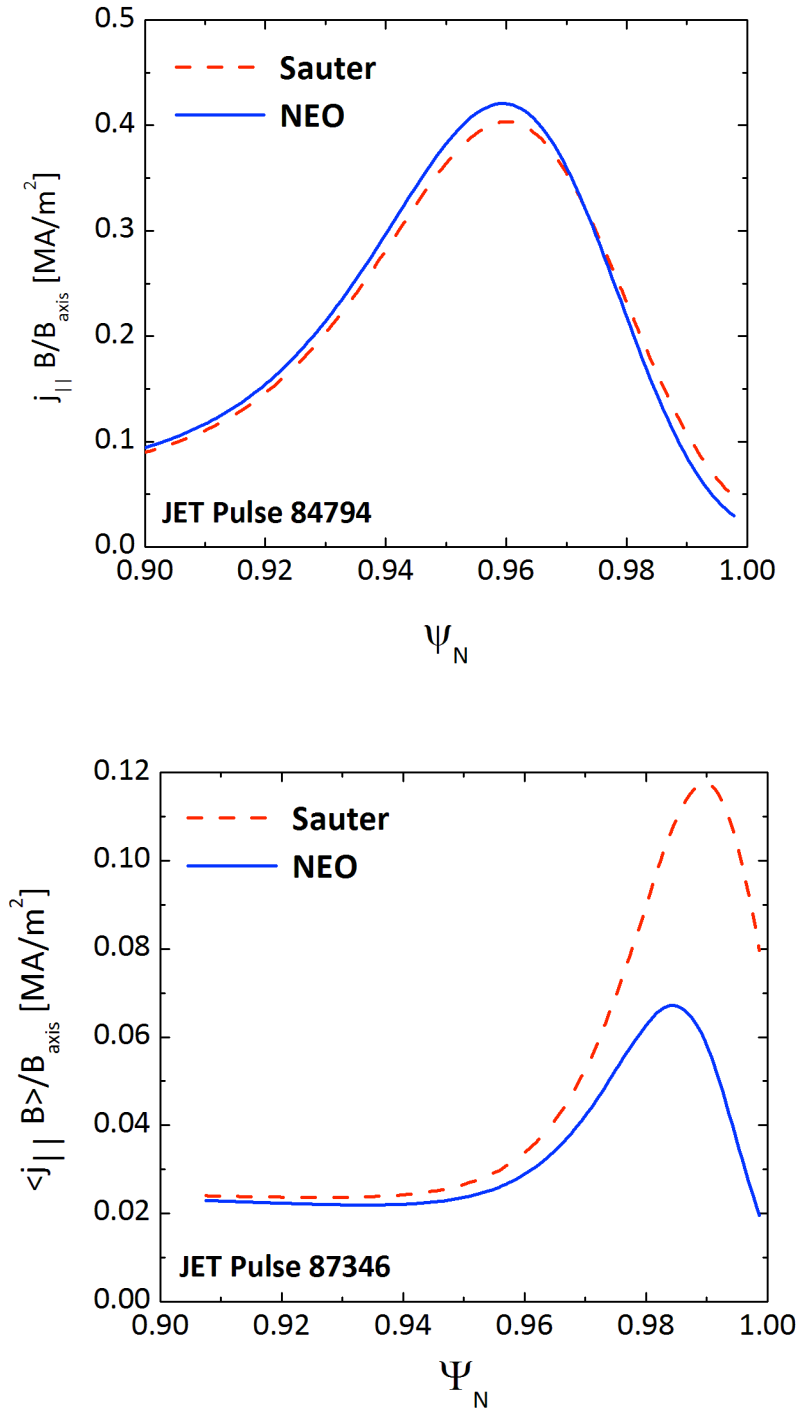


**FIGURE 10.** Comparison of edge bootstrap current profiles calculated with Sauter’s formula [12] and with NEO [15],[16] for the JET pedestals **(a)** at low gas, high power (#84794) and **(b)** at high gas, low power (#87346), this being the case with the lowest  $j_{BS}$  of the power and gas scans. The two calculations agree well at low collisionality (case [a]), except near the separatrix, whereas at high collisionality (case [b]) the Sauter calculation overestimates that from NEO by almost 100%.

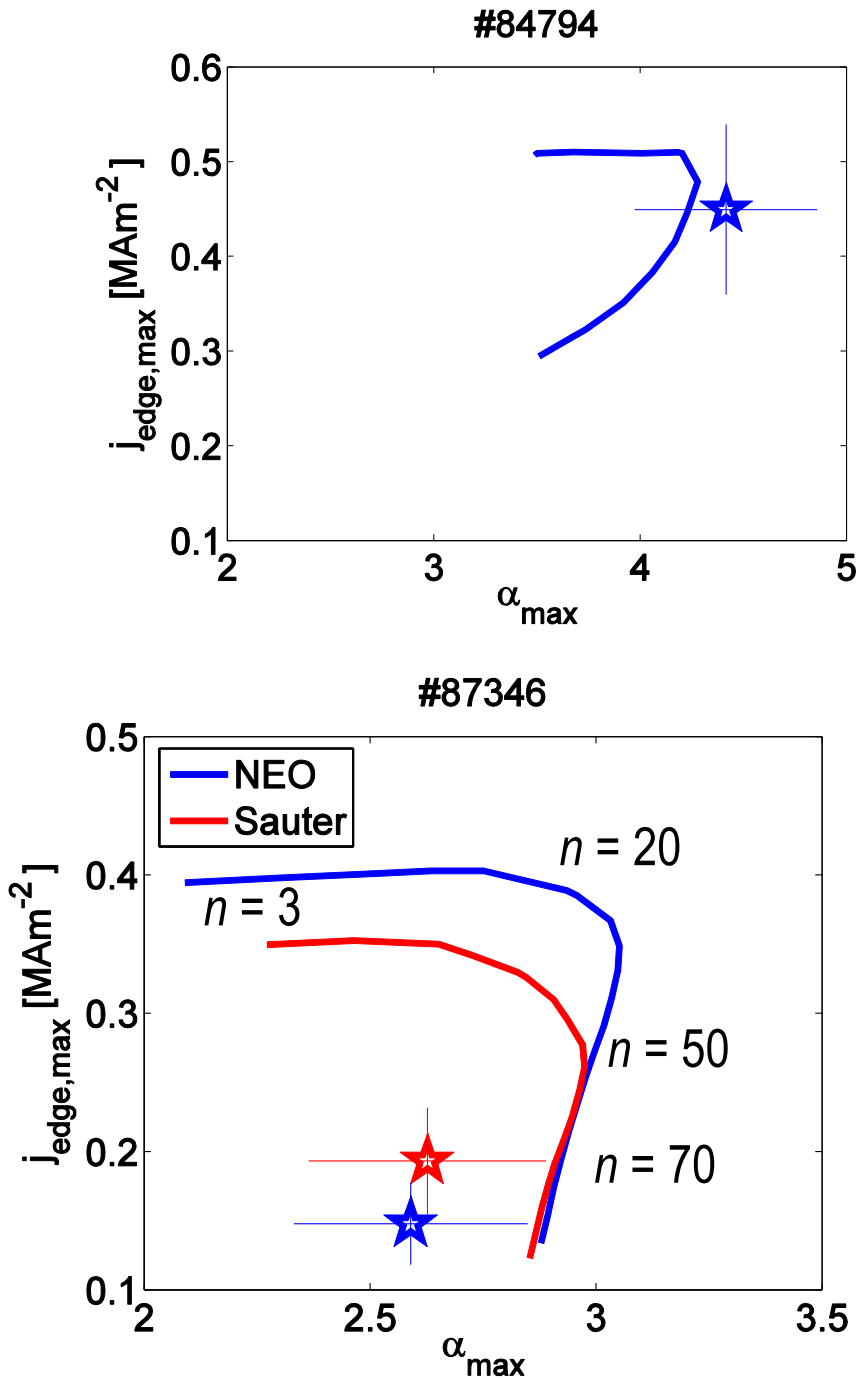


**FIGURE 11.** Comparison of the effect of  $j_{BS}$  model, Sauter (red) and NEO (blue), on the pedestal stability analysis for: **(a)** low gas, high power case #84794 (= low collisionality) where the two models are not distinguishable in the edge stability analysis and **(b)** high gas, low power pedestal #87346 (high collisionality). The ELITE calculations were run with  $n_{max} = 70$  and  $\gamma > 0.03 \omega_A$ .

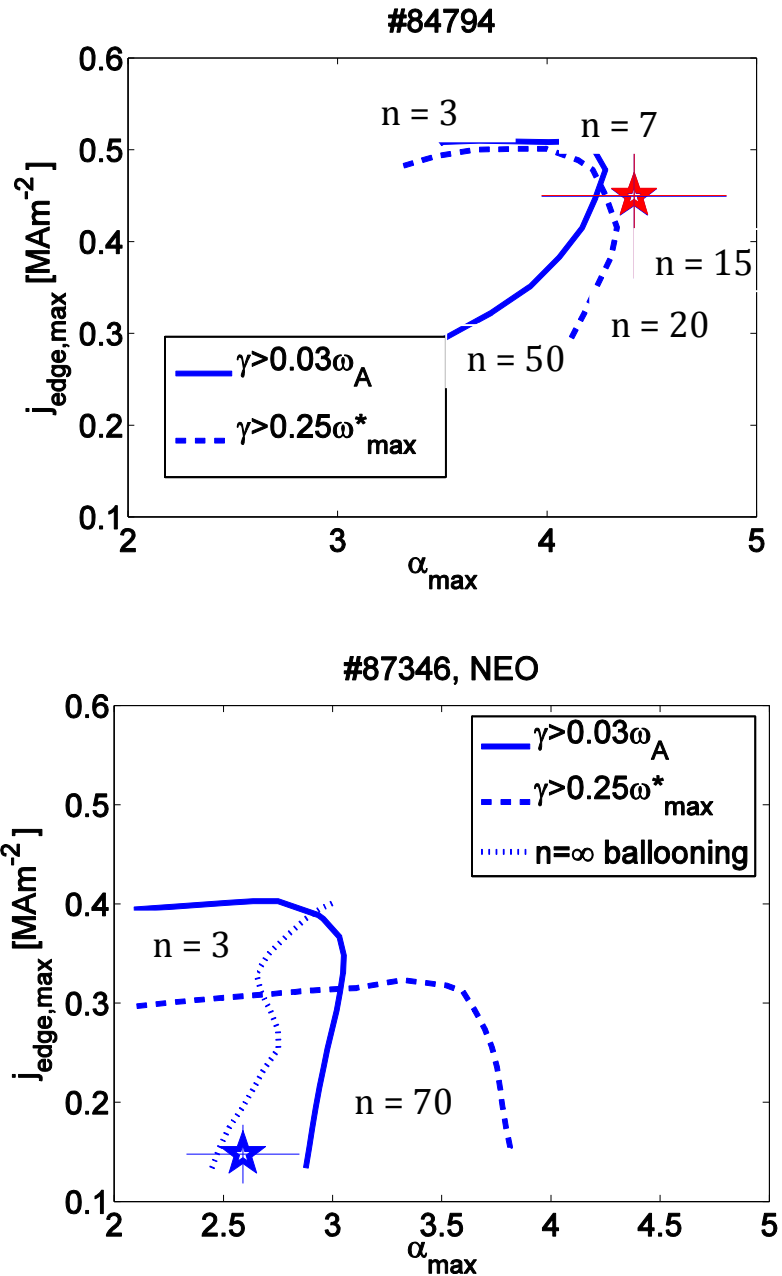


**FIGURE 12.** Effect of the choice of stability criterion for the P-B boundary on the pedestal stability analysis: **(a)** low gas/high power case (#84794, low collisionality), where the Sauter and NEO bootstrap current calculations are in very good agreement, showing no difference in the operational point, but expansion of the ballooning boundary when  $\gamma > 0.25 \omega_{\text{max}}^*$  is used; **(b)** high gas/low power pedestal (#87346, high collisionality) with  $j_{\text{BS}}$  from NEO. The  $n = \infty$  ballooning boundary is also indicated, for comparison.

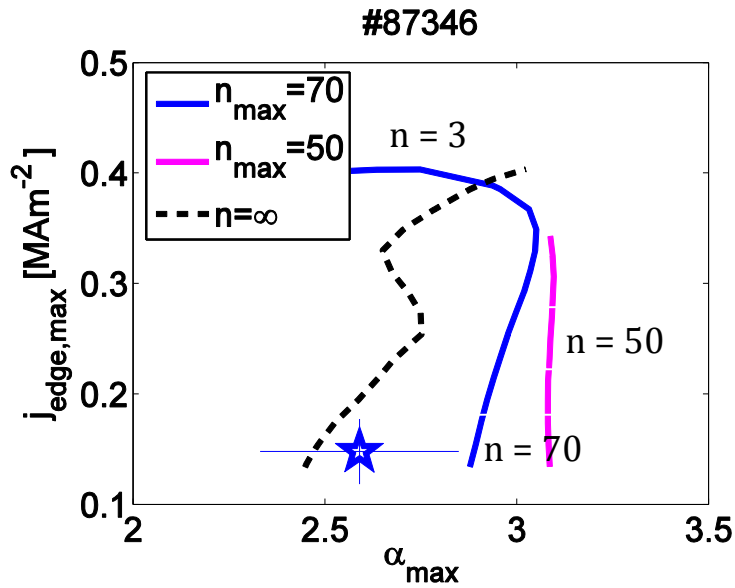


**FIGURE 13.** Sensitivity test of the choice of  $n_{\max}$  in the ELITE calculations for the high gas/low power pedestal (#87346, high collisionality), with  $\gamma > 0.03 \omega_A$  (solid boundary) and  $\gamma > 0.25 \omega_{\max}^*$  (dashed boundary) stability criteria:  $n_{\max} = 70$  (blue) and  $n_{\max} = 50$  (magenta), with  $j_{BS}$  from NEO.

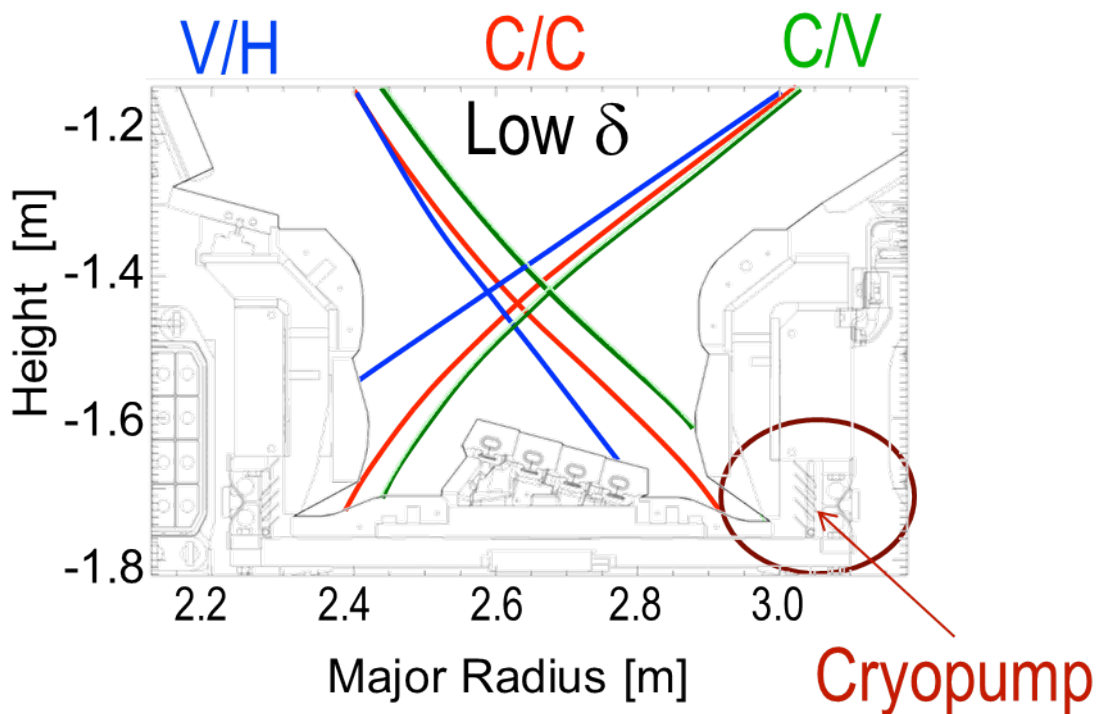


**FIGURE. 14.** Divertor configurations used in the JET-ILW pedestal studies at low, average  $\delta$  and constant main plasma shape, with MkII-HD divertor geometry: from left to right V/H (blue), C/C (red), C/V (green). The location of the divertor cryopump is also indicated.



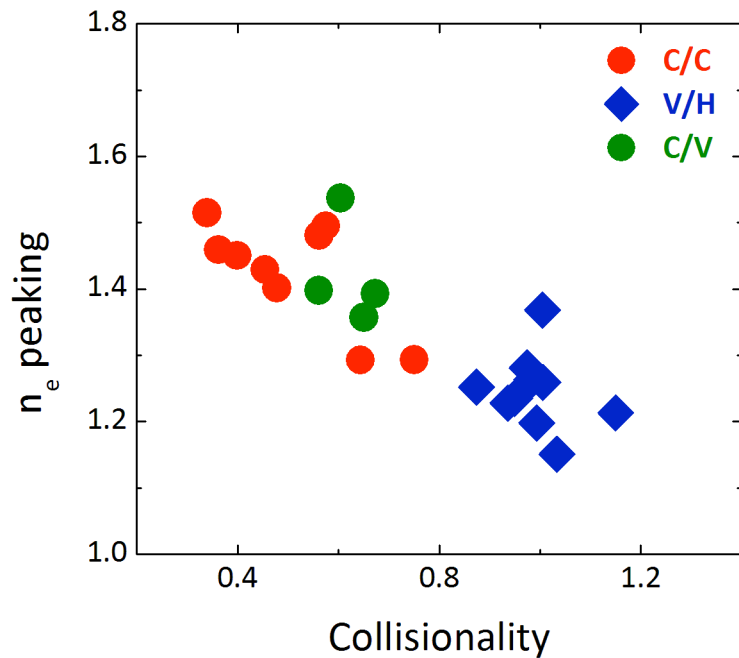
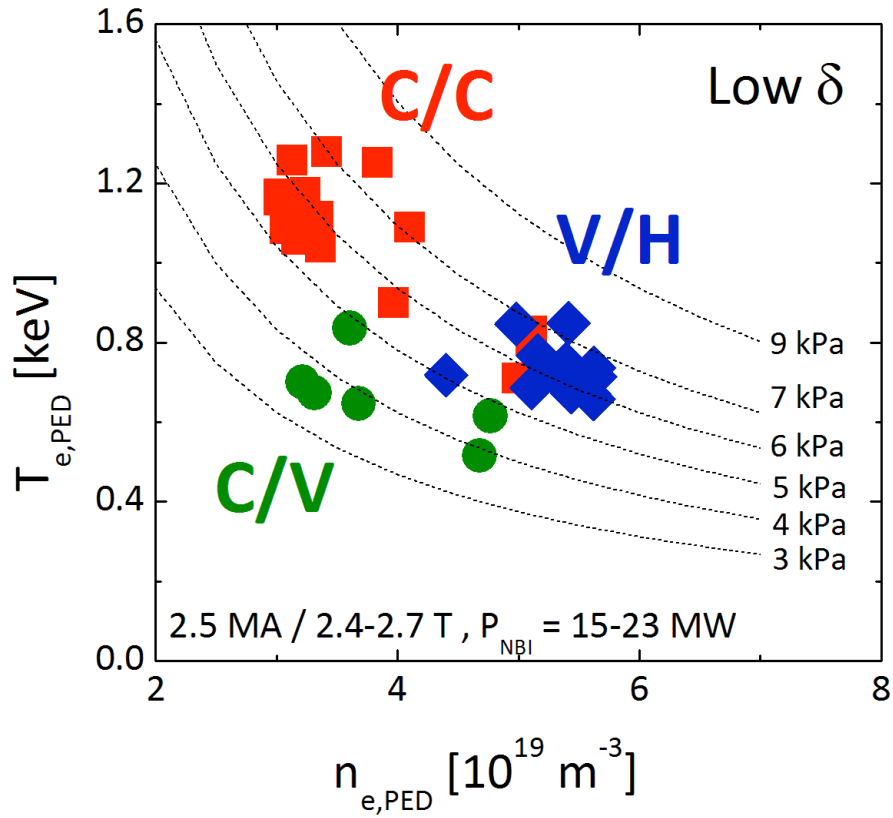


**FIGURE 15. (a)**  $n_{e,PED}$ - $T_{e,PED}$  diagram for the low  $\delta$  ELMy H-mode experiments addressing the effect of varying divertor configuration on confinement: C/C (red squares), V/H (blue diamonds) and C/V (green circles) configurations at 2.5MA/2.4-2.7T and  $P_{NBI} = 15-23 \text{ MW}$ ; **(b)** density peaking factor vs average collisionality for the same discharges.

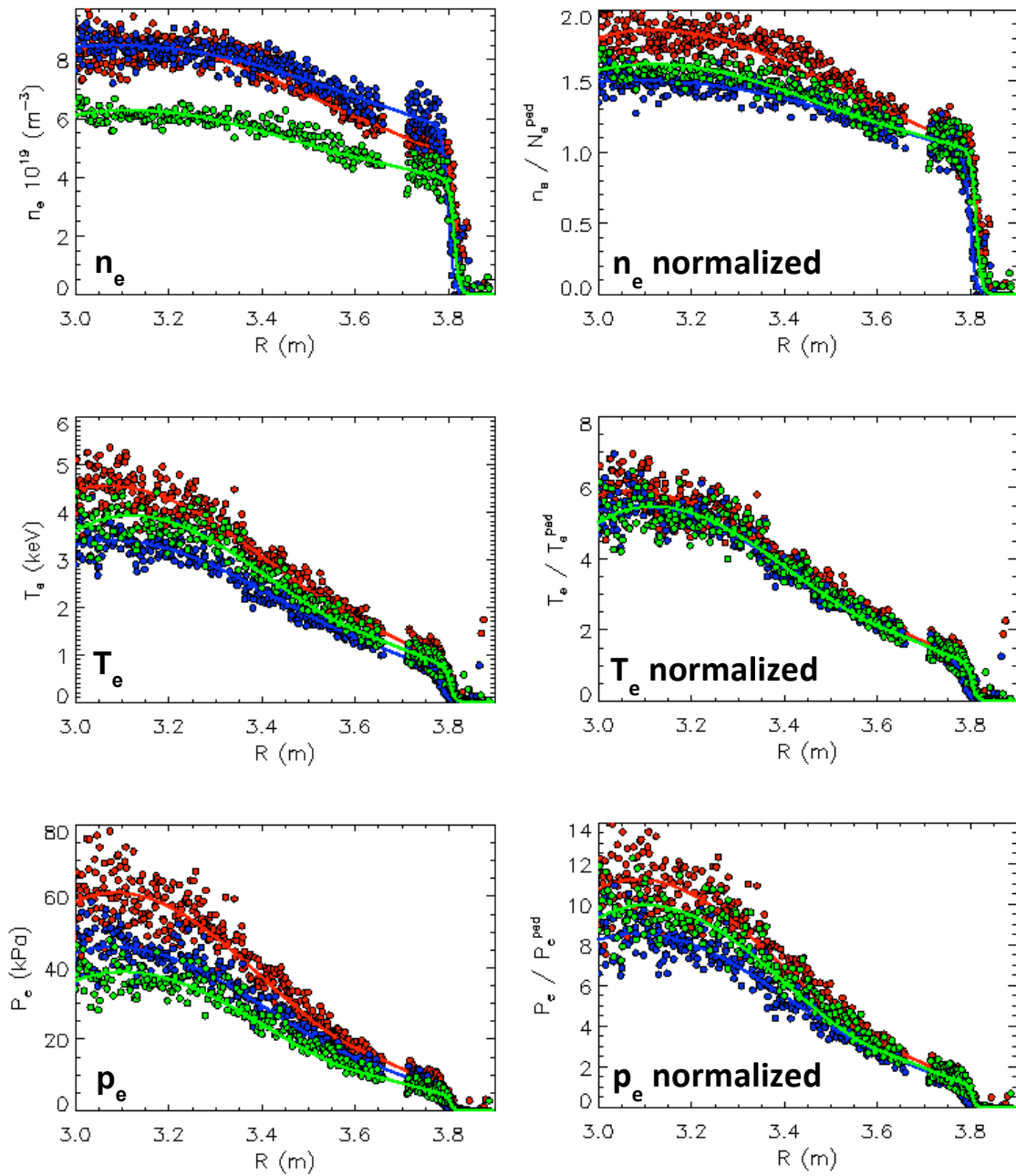


**FIGURE 16.** From top to bottom, ELM averaged radial profiles of electron density, temperature and pressure from HRTS (left panels) and correspondig profiles normalized to pedestal top values (right panels) for three selected discharges of Figure 15, at same  $P_{\text{NBI}} = 23$  MW and  $D_2$  gas rate =  $2 \times 10^{22}$  e/s, and with different divertor configurations: C/C (red), V/H (blue) and C/V (green).